iScience

CellPress
OPEN ACCESS

Article

Facile synthesis of super-thermal insulating polyimide aerogel-like films

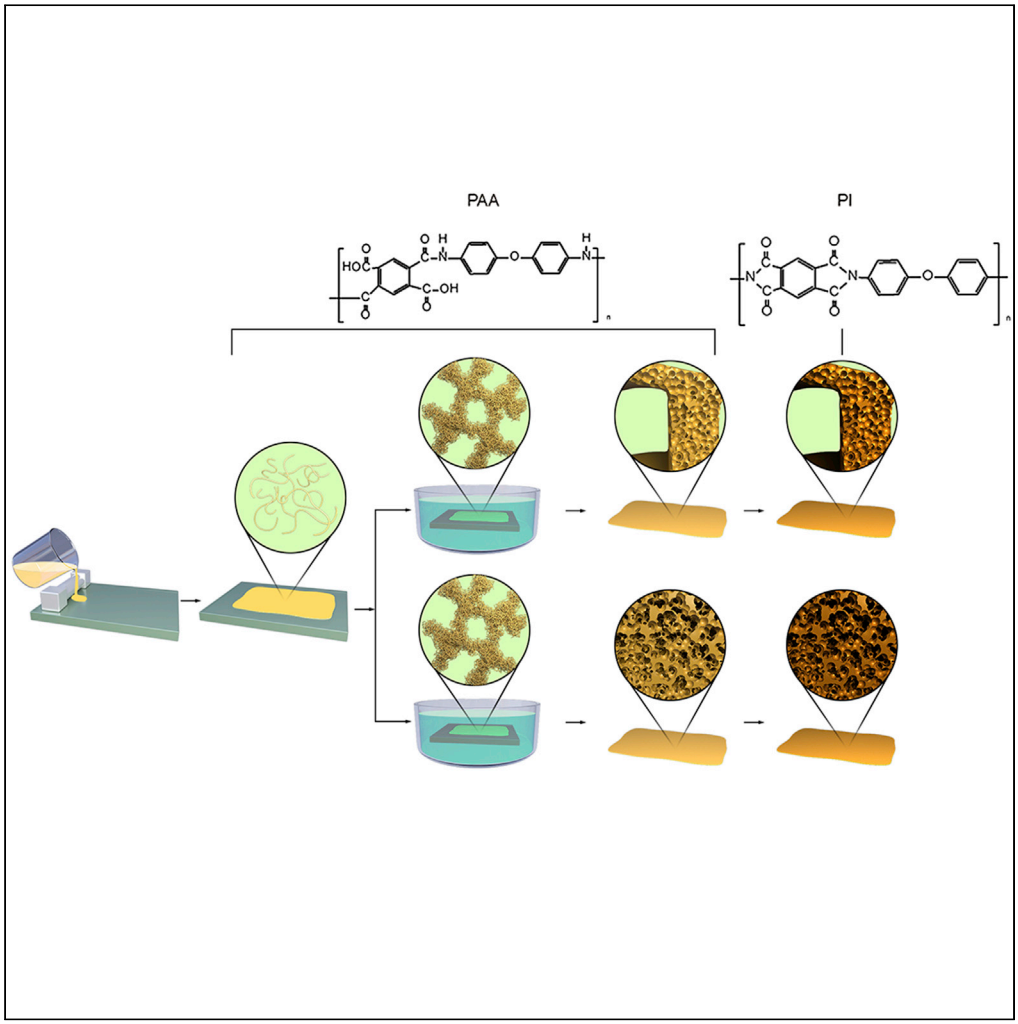

Jing Ma, Yonghui Lü, Hua Wen, ..., Lei Jiang, Lihong Liu, Shaomin Liu

qingt@buaa.edu.cn (G.Q.)
liushaomin@mail.buct.edu.cn (S.L.)

Highlights

A polyimide aerogel-like film is obtained by phase inversion and ambient drying

PI film shows low thermal conductivity values

The film has high tensile strength and high toughness

The developed porous films can be applied for thermal insulation

Ma et al., iScience 25, 105641
December 22, 2022
https://doi.org/10.1016/j.isci.2022.105641

iScience

CellPress
OPEN ACCESS

Article

Facile synthesis of super-thermal insulating polyimide aerogel-like films

Jing Ma,[1] Yonghui Lü,[1] Hua Wen,[1] Yupei Zhang,[1] Wei Wei,[2] Guotong Qin,[1,6,*] Yong Zhao,[3] Lei Jiang,[3] Lihong Liu,[4] and Shaomin Liu[5,*]

SUMMARY

Thermal superinsulation materials play a key role in reducing energy consumption. In this article, flexible polyimide aerogel-like films are developed by a facile non-solvent-induced phase separation combined with ambient drying method. The pore structure and insulation properties are well controlled by changing the compositions of the coagulation bath. Polyimide films with macro-nano hierarchical pore structure and uniform nanopores are prepared by adjusting the content of water and alcohol as the non-solvent. The relationship between the insulation performance and textured structure of polyimide was studied. After optimization, the produced film achieved a low thermal conductivity of 0.019 $W \cdot m^{-1} \cdot K^{-1}$ but good tensile strength of 89.6 MPa, compared favorably with literature results. Hence, this article demonstrates that application of the facile phase inversion method to prepare porous polymers can be expanded from desalination or gas separation fields to insulation for energy-saving purposes.

INTRODUCTION

The energy crisis and environmental deterioration are the greatest challenges facing humankind. To battle these issues, considerable efforts have been paid on application of renewable energy sources. On the other hand, reducing energy consumption is also equally important as this reduces energy requirement burden, but receiving less attention. Among various energy consumption categories, thermal energy accounts for a large proportion. Adopting superthermal insulation is a promising strategy to reduce thermal energy consumption.[1,2] For this purpose, aerogels have attracted intensive attention because of their ultralow thermal conductivity (λ) values.[3,4] In contrast to conventional insulation materials typically having λ in the range of 30–40 $W \cdot m^{-1} \cdot K^{-1}$, opacified silica aerogel has thermal conductivity as low as 0.017 $W \cdot m^{-1} \cdot K^{-1}$.[5] Resorcinol-formaldehyde aerogel even lowers the λ value to 0.012 $W \cdot m^{-1} \cdot K^{-1}$.[6] The ceramic aerogel composites containing nanoporous silica aerogel and aluminoborosilicate ceramic nanofiber possess thermal conductivity of 0.0224 $W \cdot m^{-1} \cdot K^{-1}$.[7] However, the application of these two aerogels is very limited because of their fragility and the complexity of the production process. To avoid the brittleness associated with these rigid materials, robust aerogels have been developed using flexible polymers. For example, polymeric aromatic isocyanate has been used to prepare the gel by supercritical carbon dioxide drying method. The resultant polyurethane aerogel displays the thermal conductivity of 0.022 $W \cdot m^{-1} \cdot K^{-1}$.[8] Polydicyclopentadiene aerogels grafted with polymethyl methacrylate can be obtained via the supercritical drying and exhibits a thermal conductivity of 0.039 $W \cdot m^{-1} \cdot K^{-1}$.[9] The mechanical strength of flexible aerogels can be further improved by using high strength polymer. Polyimide (PI) is a high-performance polymer with applications in a wide temperature range (-200-400°C) and with intrinsically low thermal conductivity and superior mechanical performance. Studies have been rarely reported on PI aerogel preparation. Although these PI aerogels are promising candidates in thermal insulation, their real applications are still restricted because of the time-consuming and high-pressure process with safety concerns. Based on supercritical drying method, many types of aerogels have been developed including PI aerogels from cross-linked poly (amic acid)[10] and ring-opening metathesis polymerization.[11] The PI aerogels prepared by supercritical drying method achieved low thermal conductivity (0.14–0.31 $W \cdot m^{-1} \cdot K^{-1}$) and high tensile strength from 0.27 to 11 MPa.[10–14] Freeze drying is another drying method to prepare aerogels. Aerogels were prepared by freeze drying including PI aerogels, elastic aerogels of cellulose-MOF,[15] super flexible boron nitrite aerogel,[16] carbon/sulfur aerogel,[17] and super elastic cellulose nanofiber aerogel.[18] The PI aerogel prepared by freeze drying displayed high thermal insulation property with thermal conductivity from 0.27 to 0.40 $W \cdot m^{-1} \cdot K^{-1}$ and high mechanical properties with tensile strength from

[1]School of Space and Environment, Beihang University, Shahe Campus, Beijing 102206, China

[2]College of Biochemical Engineering, Beijing Union University, Beijing 100023, China

[3]School of Chemistry, Beihang University, Beijing 100191, China

[4]WA School of Mines: Minerals, Energy and Chemical Engineering, Curtin University, Perth, WA 6102, Australia

[5]State Key Laboratory of Organic-Inorganic Composites, College of Chemical Engineering, Beijing University of Chemical Technology, Beijing 100029, China

[6]Lead contact

*Correspondence: qingt@buaa.edu.cn (G.Q.), liushaomin@mail.buct.edu.cn (S.L.)

https://doi.org/10.1016/j.isci.2022.105641

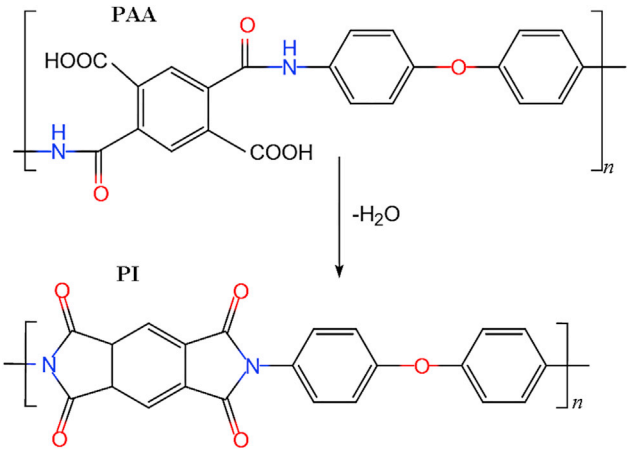

Scheme 1. The chemistry of thermal imidization process of PAA to obtain PI films

0.0052 to 5.2 MPa.[19–24] Generally, the preparation steps for these aerogels include sol-gel polymerization, solvent-exchange, and control drying (supercritical drying or freeze drying); the overall process is slow requiring a few days. In these conventional techniques, the supercritical or freezing drying method is needed to overcome the mechanical stress otherwise the collapse of the pore structure would occur. The complex process and high pressure requirement severely limits the productivity and greatly increases the cost. It is vital to develop a simple route to prepare aerogels for super-thermal insulation. Phase separation or inversion technique has been widely applied for nearly 60 years to prepare various porous polymeric membranes for desalination purposes inspired by the invention from Dr. Srinivasa Sourirajan.[25,26] Dr. Sourirajan were commented by Roberto Goizueta Professor, Menachem Elimelech, in Yale University that he should have received two Nobel Prizes – one for science and one for peace because his pioneering work had inspired a multicontinental major, the global membrane separation market worth $50.3 billion USD in 2021 to nourish life by providing accessible clean water worldwide.[27,28] However, the application of Dr. Sourirajan's method to prepare porous polymeric film for insulation to save energy consumption is rarely reported. The techniques to prepare porous membranes for separation cannot be simply borrowed to prepare thin films for insulation purpose as the former requires the porous structure in thorough connectivity but the latter requires the presence of more closed pores.

Herein, we report the phase inversion and ambient drying method to prepare polyimide aerogel-like films with super low thermal conductivity and high mechanical property (Scheme 1). In this method, the tedious procedures of solvent exchange and high pressure supercritical drying normally encountered in conventional processes are no longer needed. An important aspect of this paper is the fundamental understanding of this phase separation method to prepare insulation films by correlating the film structure, thermal conductivity and mechanic properties. The porous film achieves a low thermal conductivity (0.019 $W \cdot m^{-1} \cdot K^{-1}$) and high tensile strength (89.6 MPa). Compared to conventional technology, this method via phase inversion has been significantly simplified, paving the way for the development of superior thermal insulation polymer films which are occupying a significant part in the global multi-billion-dollar insulation market.

RESULTS AND DISCUSSION

The porous structure is formed during the phase separation process induced by the non-solvent. PI films in different thickness with hierarchal or homogeneous pore structure can be achieved just by manipulating the compositions of the coagulation solution. In this phase separation process, the composition of non-solvent plays a vital role in the final porosity of the formed PI aerogel (Figure 1). When pure water was used as the non-solvent, the resultant films showed typical hierarchical porosity featuring by dense mesoporous skin-layer, macroporous core, and thick skeletal framework with uniform nanopores (Figure 1A). The effects of the ethanol content on the pore structure of the PI films were investigated by adding ethanol into water at an increasing step of 10%. The gradual evolution of the morphology of the PI films is shown in Figures 1 and S1. For comparison, a PI film obtained by solvent evaporation was also examined, which showed a nonporous structure (Figure S1L). Addition of 20% ethanol in the coagulation bath reduced the number

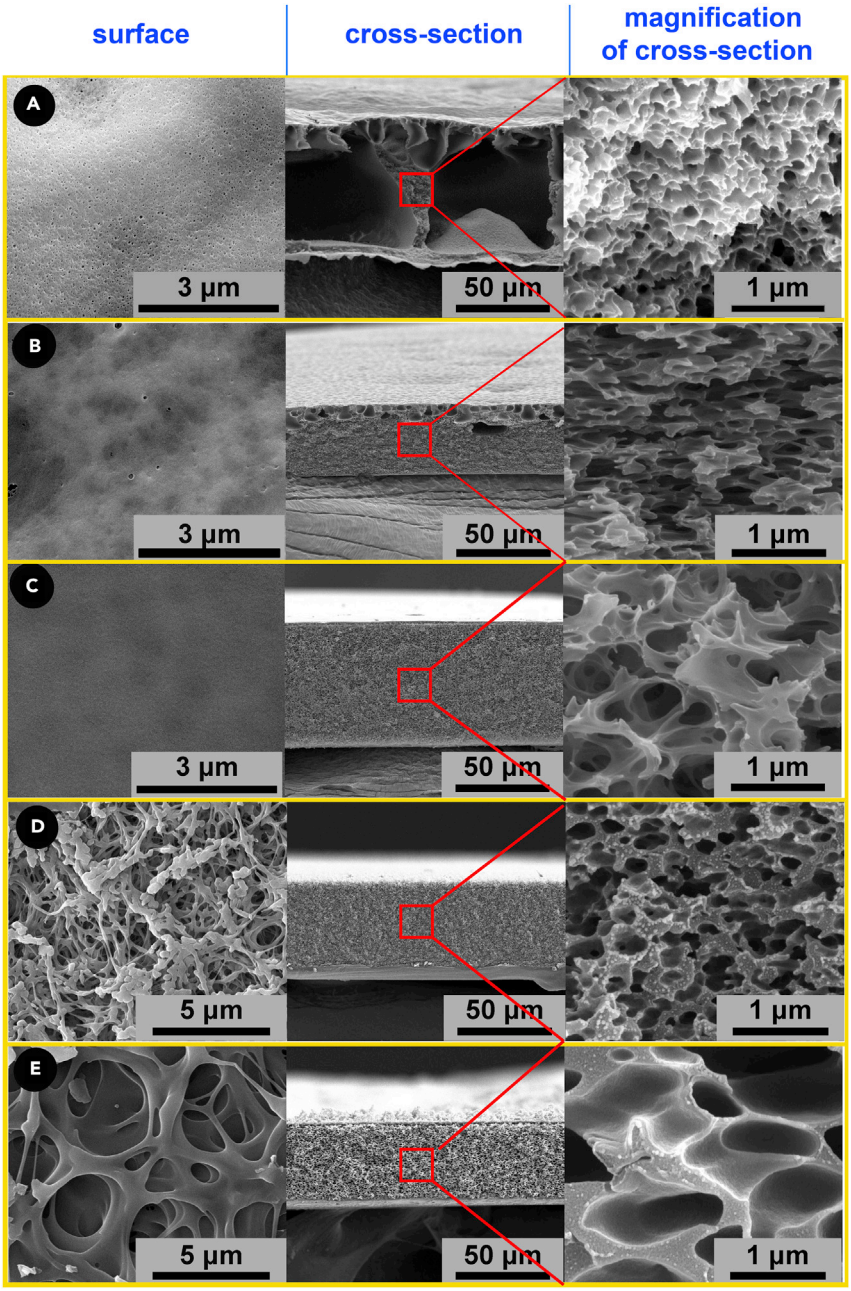

Figure 1. Morphologies and microstructures of polyimide films from coagulation baths comprising different ethanol and water ratios

Samples from a to e were obtained from coagulation baths containing pure water, 80% water/20% ethanol, 60% water/40% ethanol, 30% water/70% ethanol; 10% water/90% ethanol, respectively. With the addition of ethanol, the macro voids disappeared and the film structure changed from hierarchal micro-nano porous to homogeneous porous whereas the surface of the film changed from slight porous to highly porous (A–C). When the ethanol content reached 70%, the pore size reduced to a minimum value (D). Further increase of ethanol in coagulation bath resulted in partially fused surface pores (E left), larger inside pores in thicker walls (E right).

and size of macro-voids (from tens of microns to hundreds of nanometers) (Figure 1B). Many of these pores are interconnected. With increasing ethanol in the coagulation bath to 40%, the macro-voids disappeared and the film became symmetric (Figure 1C). The interconnectivity of pores gradually decreased with the increase of ethanol content in coagulation bath. On further increasing the ethanol content up to 70%,

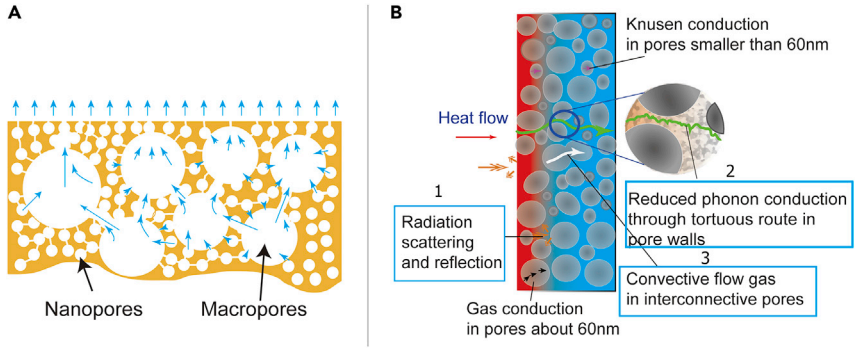

Figure 2. Safe drying strategy (A) and insulation mechanisms (B) of hierarchical PI aerogels

(A) The tunnels between large pores allow the solvent vapor to escape uninhibited. The thin wall skeletons reduce stress from drying of small pores, leading to a safe drying process without pore collapse.

(B) The reduced heat radiation is because of the reflection and scattering on the interfaces of the pore walls (1). The phonon conduction is also reduced because of the highly tortuous transport route along with the pore walls (2). Heat transfer by convective flow gas only occurs in large and connected pores (3). The heat conduction via hot gaseous transport is reduced by the pores with low interconnectivity (preventing convective flow gas).

the frame walls became thicker and the pore size decreased with lower interconnectivity (Figure 1D). The film made from the coagulation bath with an ethanol content of 70% produced the smallest pores. When the ethanol content reached 90%, the pore walls became thicker and the pore size was enlarged (Figure 1E). Most of the structural differences in the phase inversion films can be rationalized in terms of the basic thermodynamic and kinetic relationships of solvent diffusion from PAA phase to non-solvent during phase separation.[29] When the homogeneous PAA casting solution is immersed in the coagulation bath, N,N-Dimethylformamide (DMF) solvent diffuses and leaves whereas non-solvent enters the film. At the interface of DMF and non-solvent, polymer precepted spontaneously because of phase separation.

When using a strong precipitant such as pure water, a dense skin with much reduced porosity immediately forms on the surface of the film (Figure 1A, left and middle). This skin-layer blocks the inward diffusion of the non-solvent and the outward diffusion of casting solvent.[30] Because of the dilution of the casting solvent by the entrapped non-solvent, phase separation of the solution beneath the skin slows down, which transforms the PAA solution to a polymer-rich phase and a polymer-lean phase (solvent-rich phase). The SEM images of the film cross-section (Figure 1) clearly show that the voids were isolated and surround by continuous polymer phase. Such a morphology formation suggests that the phase separation underwent a process of nucleation and growth of solvent-rich phase.[31] The solvent-rich phase gradually grew up with the non-solvent penetration through the surrounding continuous polymer-rich phase. The interfacial boundary between the polymer-rich phase and the solvent-rich phase gradually transferred to polymer-rich phase, and the formed macrovoids were originated from the solvent-rich phase. On the other hand, the polymer-rich phase transformed to a solid phase. During solidification, phase separation continues to complete within the polymer-rich phase, leading to the yield of nanoporous structure. A hierarchical micro-nano interlocking structure was thus formed. When ethanol was added into the coagulation bath, the non-solvent was not as strong as pure water. This resulted in a higher affinity between PAA and non-solvent, slowing down the phase separation rate. Therefore, skin-layer phase separation was retarded from initially and instantaneously fast rate,[21] thus the surface of the film became porous (Figures 1D and 1E left). The porous skin exerted a lower resistance to the diffusion of solvent and non-solvent, therefore the phase separation inside the film bulk occurred in a shorter period. The solvent-rich phase could not be sufficiently expanded because the fast non-solvent diffusion leads to the solidification of polymer-rich phase or the formed film with homogeneous porous structure consisting of smaller and more closed pores. The further increase of ethanol in coagulation bath resulted in partially fused structure on the skin which might enhance the diffusion resistance of the solvent and non-solvent. Furthermore, the higher affinity between the PAA and the non-solvent resulted in delayed phase separation inside the film bulk, producing thicker solid walls and enlarged pores. The gradual morphology evolution of the film is shown in Figure S1. The hierarchical pore structure is beneficial to reduce the drying stress, providing a quick pathway for solvent removal (Figure 2A). The drying stress is related with the film thickness and porous structure. The interconnected tunnels between the large pores accelerated the movement of water vapor

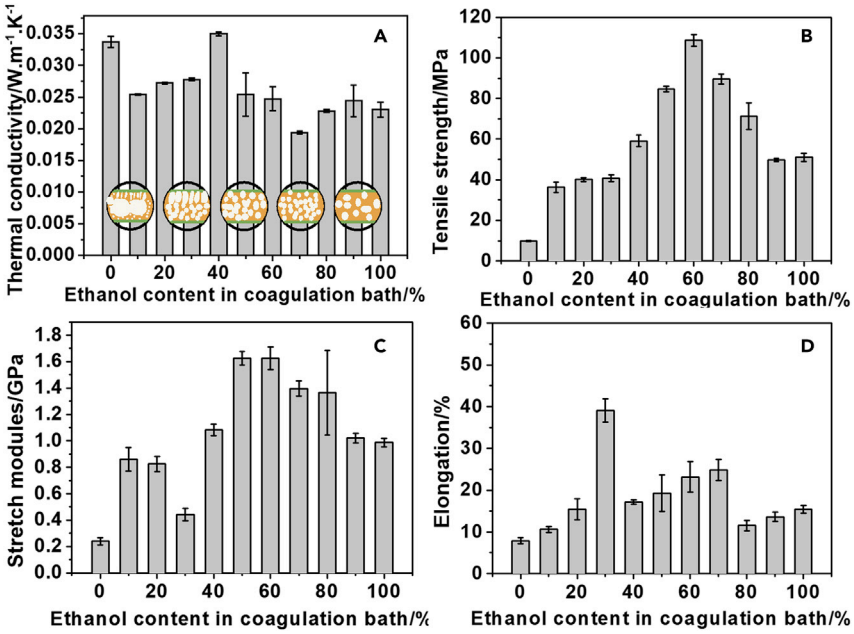

Figure 3. Effects of ethanol content in the coagulation bath on the thermal conductivities (A) and mechanical performances (B–D) of polyimide aerogel-like films. The error bars indicate standard deviations.

therefore improved the moisture distribution in the thickness direction and decreased the drying stress. Enormous local surface tension originates from drying of the small pores in the walls of large pores. However, the local drying stress is kept at a low level by controlling drying layer in the small thickness (thin pore walls), maintaining the pore structure well during drying process.[32] The film thermal conductivity is closely related to pore structure (Figure 2B). Pore size and connectivity and tortuosity of phonon transport path jointly determine the thermal conductivity of porous materials. Fortunately, just by changing the composition of the non-solvent, we can optimize the pore structure of film to realize ultralow thermal conductivity.

With increasing ethanol content in the coagulation bath, thermal conductivity of the PI films gradually changed (Figure 3A). When pure water was used as non-solvent, the PI film showed a thermal conductivity of 0.034 $W \cdot m^{-1} \cdot K^{-1}$. The high porosity and small pores of the film provide a tortuous route along the skeleton for thermal conduction leading to the decreased thermal conductivity based on phonon vibration (Figure 2). Although the solid conductivity was reduced because of the presence of nanoporous walls, the gas trapped in the macrovoids should contribute significantly to the heat transfer (Figure 2A). When the pore size is smaller than the free path of the air (about 70 nm), the gas contribution to the thermal conductivity is mainly through Knudsen diffusion and static gas conduction (Figure 2B). When the pore size is larger than the mean free path of the air, like the macrovoids in the films made from pure water coagulation, the gas convective flow occurs in the pores, leading to the enhanced thermal conduction.

With the increment of ethanol in coagulation bath, the thermal conductivity of PI film decreased because of the reduced large macro pores (or voids) (Figures 1A, 1B, and S1A–S1D). The exceptional high conductivity of 0.035 $W \cdot m^{-1} \cdot K^{-1}$ for the film from coagulation containing 40% ethanol might be related with its large and interconnected pores to contribute to fast thermal transferring by gas convective flow conduction. The minimum thermal conductivity of 0.019 $W \cdot m^{-1} \cdot K^{-1}$ was reached by the film obtained from the coagulation bath containing 70% ethanol, corresponding to its smallest pores mostly in closed structure (Figures 1D and S1H) effectively reducing the gas/phonon thermal transferring. The achieved minimum thermal conductivity is comparable to 0.014 $W \cdot m^{-1} \cdot K^{-1}$ of PI aerogels obtained by the complex sol-gel process involving supercritical drying.[6] The further increase of ethanol in coagulation resulted in the film with enlarged pores and thick pore walls (Figure S1). As discussed above, the larger pore walls increased gas thermal conduction via convective flow. The thicker walls and large pores

Table 1. Textural characteristics of PI films

Ethanol content in coagulation (%)	Density ($g \cdot cm^{-3}$)	Porosity I (%)[a]	Surface area ($m^2 \cdot g^{-1}$)	Total pore volume ($cm^3 \cdot g^{-1}$)	Porosity II (%)[b]
0	0.7715	42.6	18.2	0.070	8.6
10	0.7081	47.3	22.0	0.077	9.4
20	0.7475	44.4	14.6	0.082	10.0
30	0.7962	40.8	14.2	0.094	11.2
40	0.9083	32.4	14.2	0.038	4.8
50	0.8970	33.3	10.1	0.045	5.6
60	0.7624	43.3	11.7	0.028	3.7
70	0.7149	46.8	14.0	0.044	5.6
80	0.8579	36.2	5.5	0.014	1.8
90	0.6457	52.0	4.7	0.014	1.9
100	0.7515	44.1	7.8	0.016	2.1

[a]Porosity I was calculated from the apparent density of the porous PI film and dense PI film.
[b]Porosity II was calculated from the pore volume from nitrogen adsorption and density of dense PI film.

lead to a shorter route for phonon conduction, thus promoting the thermal conduction via phonon vibration (Figure 2A). The thermal conductivity of the PI film was 0.024 $W \cdot m^{-1} \cdot K^{-1}$ when absolute ethanol was used as the non-solvent to prepare the film.

The measured tensile strength and modulus of the films confirm their high mechanical performance (Figures 3B–3D). The film with the lowest thermal conductivity also processed a relatively high strength of 89.6 MPa, a modulus of 1.39 GPa, and an elongation ratio of 25%. These results might be related with the uniform pore size of the film from the coagulation with 70% ethanol. Actually, all the films from the coagulation bath with 50-80% ethanol gave relatively high tensile strength (Figure 3B), high stretch modulus (Figure 3C) and high elongation (Figure 3D). This implies that PI films with high performance for superthermal insulation can be flexibly prepared in wide range composition of coagulation bath. All films show superior thermal stability and can be stable up to 400°C in nitrogen (as shown in Figure S2).

Because of the superior toughness and tensile strength, these PI films can be folded into multiple layers. IR image analysis can be applied to detect the change of thermal insulation property of PI films. As observed from Figure S3, the surface temperature of PI films gradually decreased with the increase of film layers. When IR image was captured immediately after placing the PI films on the hot stage, the surface temperature was decreased from 40.6 to 22.8°C for the film thickness increased from 1 to 48 layers. On the other hand, the surface temperature of PI films (48 layers) was slowly improved from 22.8 to 28.7°C as indicated by IR images captured at 0 to 600 s, respectively. All these observations highlight the effective thermal insulation property of the resultant PI films.

All the porous PI films exhibited quite low thermal conductivities varied from 0.019 to 0.035 $W \cdot m^{-1} \cdot K^{-1}$, correlating with their respective porous structures. Table 1 gives the textural information of these porous films. Figure S4 shows the effects of ethanol content in coagulation on the nitrogen adsorption isotherms and pore size distributions of aerogel PI films. The porosity I (32.4–52.0%) from apparent density of porous and dense films shows the total porosity including the closed pores and open pores. The porosity II (1.9–11.2%) from the pore volume based on nitrogen adsorption reflects the open pores only. The differences between porosity I and porosity II indicate that most pores in porous PI films are closed, beneficial to lowering the thermal conductivity. In Figure S4, the variation trends of nitrogen adsorption isotherms and pore size distributions were not in high accordance with SEM observation. For example, high porosity and uniform pore size are shown in Figure 1D, but not reflected in Figure S4. This phenomenon implies that large fraction of pores is closed in the resultant aerogel PI films made from the ethanol content of 70% in coagulation bath. The variation trend of porosity I and II, surface area, nitrogen adsorption and pore size distributions was not consistent with the thermal conductivity change,

indicating that the conductivity was affected by other factors more than porosity solely. The lowest thermal conductivity is associated with the uniform nanopores and highly closed porosity (striking difference between porosity I of (46.8%) and, porosity II (5.6%)), mirroring the pore structure is playing the key role in affecting the thermal conductivity. Noteworthy that the film with lowest thermal conductivity also has a quite high tensile strength, modulus and thermal stability, indicating that the uniform nanoporous structure is also favorable to enhance the mechanic performance for applications at various temperatures.

Limitations of the study

In this work, we prepared the polyimide aerogel-like films for super-thermal insulation just by adjusting the relative content of water and ethanol in the non-solvent for polymer phase separation. The developed polyimide films possess the ideal micro-nano hierarchical pore structure, conferring not only the lowest thermal conductivity but also a high tensile strength, modulus and thermal stability. Nevertheless, this approach is limited to the thin sample thickness. The phase separation method is closely related with the mass transfer rate, which is strongly affected by the sample thickness. If the film samples are too thick (for example, larger than 1 mm), the described uniform porous structure cannot be guaranteed, which may pose a limitation to these applications where thick films are required. Fortunately, a thin film can be folded into a thick one with multiple layers. Film folding may help to find more application scenarios.

STAR★METHODS

Detailed methods are provided in the online version of this paper and include the following:

- KEY RESOURCES TABLE
- RESOURCE AVAILABILITY
  - Lead contact
  - Materials availability
  - Data and code availability
- EXPERIMENT MODEL AND SUBJECT DETAILS
  - Preparation of films
  - Effects of the coagulation composition on the structure of PI films
  - Thermogravimetric stability
  - Heat transferring property of the aerogel PI films
  - The weight loss, area shrinkage and thickness change before and after drying or imidization
- METHOD DETAILS
  - Thermal conductivity measurement
  - Tensile performance measurement
  - Surface morphology
  - BET surface area, pore volume, and pore size measurement
  - Infrared thermal images
  - Thermogravimetric analysis
- QUANTIFICATION AND STATISTICAL ANALYSIS

SUPPLEMENTAL INFORMATION

Supplemental information can be found online at https://doi.org/10.1016/j.isci.2022.105641.

ACKNOWLEDGMENTS

Supported by National Natural Science Foundation of China (52070009, 52000006, 51772031), the China Postdoctoral Science Foundation (2020TQ0026), the National Basic Research Program of China (2012CB933201, 2010CB934700) and the Fundamental Research Fund for the Central University (Buctrc202115).

AUTHOR CONTRIBUTIONS

J.M., W.W., and G.Q. proposed the conceptualization. J.M., Y.L., H.W., and Y.Z. performed the formal analysis. J.M., Y.L., H.W., and Y.Z. performed investigation and methodology. G.Q. supervised the data analysis and article writing. The original draft was written through contributions of J.M. and G.Q. W.W., G.Q., Y.Z., L.J., S.L., and L.L. performed review and editing. All authors have given approval to the final version of the manuscript.

DECLARATION OF INTERESTS

The authors declare no competing interests.

Received: July 28, 2022
Revised: October 5, 2022
Accepted: November 17, 2022
Published: December 22, 2022

REFERENCES

1. Apostolopoulou-Kalkavoura, V., Hu, S., Lavoine, N., Garg, M., Linares, M., Munier, P., Zozoulenko, I., Shiomi, J., and Bergström, L. (2021). Humidity-dependent thermal boundary conductance controls heat transport of super-insulating nanofibrillar foams. Matter *4*, 276–289. https://doi.org/10.1016/j.matt.2020.11.007.

2. Kim, J.Y., and Jia, X. (2020). From space to battlefield: a new breed of multifunctional fiber sheets for extreme environments. Int. J. Radiat. Oncol. Biol. Phys. *3*, 602–604. https://doi.org/10.1016/j.matt.2020.08.016.

3. Chen, C., and Hu, L. (2019). Super elastic and thermally insulating carbon aerogel: go tubular like polar bear hair. Matter *1*, 36–38. https://doi.org/10.1016/j.matt.2019.06.012.

4. Gonzalez, G.M., Ward, J., Song, J., Swana, K., Fossey, S.A., Palmer, J.L., Zhang, F.W., Lucian, V.M., Cera, L., Zimmerman, J.F., et al. (2020). para-Aramid fiber sheets for simultaneous mechanical and thermal protection in extreme environments. Matter *3*, 742–758. https://doi.org/10.1016/j.matt.2020.06.001.

5. Hümmer, E., Rettelbach, T., Lu, X., and Fricke, J. (1993). Opacified silica aerogel powder insulation. Thermochim. Acta *218*, 269–276. https://doi.org/10.1016/0040-6031(93)80428-D.

6. Lu, X., Arduini-Schuster, M.C., Kuhn, J., Nilsson, O., Fricke, J., and Pekala, R.W. (1992). Thermal conductivity of monolithic organic aerogels. Science *255*, 971–972. https://doi.org/10.1126/science.255.5047.971.

7. An, L., Wang, J., Petit, D., Armstrong, J.N., Hanson, K., Hamilton, J., Souza, M., Zhao, D., Li, C., Liu, Y., et al. (2020). An all-ceramic, anisotropic, and flexible aerogel insulation material. Nano Lett. *20*, 3828–3835. https://doi.org/10.1021/acs.nanolett.0c00917.

8. Biesmans, G., Randall, D., Francais, E., and Perrut, M. (1998). Polyurethane-based organic aerogels' thermal performance. J. Non-Cryst. Solids *225*, 36–40. https://doi.org/10.1016/s0022-3093(98)00103-3.

9. Mohite, D.P., Mahadik-Khanolkar, S., Luo, H., Lu, H., Sotiriou-Leventis, C., and Leventis, N. (2013). Polydicyclopentadiene aerogels grafted with PMMA: II. Nanoscopic characterization and origin of macroscopic deformation. Soft Matter *9*, 1531–1539. https://doi.org/10.1039/C2SM27606B.

10. Guo, H., Meador, M.A.B., McCorkle, L., Quade, D.J., Guo, J., Hamilton, B., Cakmak, M., and Sprowl, G. (2011). Polyimide aerogels cross-linked through amine functionalized polyoligomeric silsesquioxane. ACS Appl. Mater. Interfaces *3*, 546–552. https://doi.org/10.1021/am101123h.

11. Leventis, N., Sotiriou-Leventis, C., Mohite, D.P., Larimore, Z.J., Mang, J.T., Churu, G., and Lu, H. (2011). Polyimide aerogels by ring-opening metathesis polymerization (ROMP). Chem. Mater. *23*, 2250–2261. https://doi.org/10.1021/cm200323e.

12. Hou, X., Mao, Y., Zhang, R., and Fang, D. (2021). Super-flexible polyimide nanofiber cross-linked polyimide aerogel membranes for high efficient flexible thermal protection. Chem. Eng. J. *417*, 129341. https://doi.org/10.1016/j.cej.2021.129341.

13. Li, X., Dong, G., Liu, Z., and Zhang, X. (2021). Polyimide aerogel fibers with superior flame resistance, strength, hydrophobicity, and flexibility made via a universal sol-gel confined transition strategy. ACS Nano *15*, 4759–4768. https://doi.org/10.1021/acsnano.0c09391.

14. Meador, M.A.B., Wright, S., Sandberg, A., Nguyen, B.N., Van Keuls, F.W., Mueller, C.H., Rodríguez-Solís, R., and Miranda, F.A. (2012). Low dielectric polyimide aerogels as substrates for lightweight patch antennas. ACS Appl. Mater. Interfaces *4*, 6346–6353. https://doi.org/10.1021/am301985s.

15. Zhou, S., Apostolopoulou-Kalkavoura, V., Tavares da Costa, M.V., Bergström, L., Strømme, M., and Xu, C. (2019). Elastic aerogels of cellulose Nanofibers@Metal–organic frameworks for thermal insulation and fire retardancy. Nano-Micro Lett. *12*, 9. https://doi.org/10.1007/s40820-019-0343-4.

16. Li, G., Zhu, M., Gong, W., Du, R., Eychmüller, A., Li, T., Lv, W., and Zhang, X. (2019). Boron nitride aerogels with super-flexibility ranging from liquid nitrogen temperature to 1000°C. Adv. Funct. Mater. *29*, 1900188. https://doi.org/10.1002/adfm.201900188.

17. Matsuura, T. (2020). Tribute to S. Sourirajan: great scientist, inventor and philosopher. Chem. Eng. Res. Des. *160*, 351–355. https://doi.org/10.1016/j.cherd.2020.05.030.

18. Qin, H., Zhang, Y., Jiang, J., Wang, L., Song, M., Bi, R., Zhu, P., and Jiang, F. (2021). Multifunctional superelastic cellulose nanofibrils aerogel by dual ice-templating assembly. Adv. Funct. Mater. *31*, 2106269. https://doi.org/10.1002/adfm.202106269.

19. Cheng, Y., Zhang, X., Qin, Y., Dong, P., Yao, W., Matz, J., Ajayan, P.M., Shen, J., and Ye, M. (2021). Super-elasticity at 4 K of covalently crosslinked polyimide aerogels with negative Poisson's ratio. Nat. Commun. *12*, 4092. https://doi.org/10.1038/s41467-021-24388-y.

20. Hou, X., Zhang, R., and Fang, D. (2020). Flexible, fatigue resistant, and heat-insulated nanofiber-assembled polyimide aerogels with multifunctionality. Polym. Test. *81*, 106246. https://doi.org/10.1016/j.polymertesting.2019.106246.

21. Qin, P., Han, B., Chen, C., Li, J., and Sun, B. (2008). Performance control of asymmetric poly(phthalazinone ether sulfone ketone) ultrafiltration membrane using gelation. Korean J. Chem. Eng. *25*, 1407–1415. https://doi.org/10.1007/s11814-008-0231-y.

22. Xue, T., Fan, W., Zhang, X., Zhao, X., Yang, F., and Liu, T. (2021). Layered double hydroxide/graphene oxide synergistically enhanced polyimide aerogels for thermal insulation and fire-retardancy. Compos. B Eng. *219*, 108963. https://doi.org/10.1016/j.compositesb.2021.108963.

23. Xue, T., Zhu, C., Feng, X., Wali, Q., Fan, W., and Liu, T. (2022). Polyimide aerogel fibers with controllable porous microstructure for super-thermal insulation under extreme environments. Adv. Fiber Mater. *4*, 1118–1128. https://doi.org/10.1007/s42765-022-00145-8.

24. Zhang, X., Li, W., Song, P., You, B., and Sun, G. (2020). Double-cross-linking strategy for preparing flexible, robust, and multifunctional polyimide aerogel. Chem. Eng. J. *381*, 122784. https://doi.org/10.1016/j.cej.2019.122784.

25. Sourirajan, S. (1963). Separation of gases by flow under pressure through porous membranes. Nature *199*, 590–591. https://doi.org/10.1038/199590A0.

26. Sourirajan, S. (1964). Separation of hydrocarbon liquids by flow under pressure through porous membranes. Nature *203*, 1348–1349. https://doi.org/10.1038/2031348a0.

27. Ismail, A.F., and Matsuura, T. (2018). Progress in transport theory and characterization method of reverse osmosis (RO) membrane in past fifty years. Desalination *434*, 2–11. https://doi.org/10.1016/j.desal.2017.09.028.

28. Orooji, Y. (2022). Father of reverse osmosis who made a huge impact on our world: srinivasa Sourirajan (October 16, 1923–February 20, 2022). npj Clean Water *5*, 20. https://doi.org/10.1038/s41545-022-00167-0.

29. Wienk, I.M., van den Boomgaard, T., and Smolders, C.A. (1994). The formation of nodular structures in the top layer of ultrafiltration membranes. J. Appl. Polym. Sci. *53*, 1011–1023. https://doi.org/10.1002/APP.1994.070530804.

30. Bottino, A., Capannelli, G., and Munari, S. (1985). Effect of coagulation medium on properties of sulfonated polyvinylidene fluoride membranes. J. Appl. Polym. Sci. *30*, 3009–3022. https://doi.org/10.1002/app.1985.070300723.

31. Nunes, S.P., and Inoue, T. (1996). Evidence for spinodal decomposition and nucleation and growth mechanisms during membrane formation. J. Memb. Sci. *111*, 93–103. https://doi.org/10.1016/0376-7388(95)00281-2.

32. Scherer, G.W. (1992). Recent progress in drying of gels. J. Non-Cryst. Solids *147–148*, 363–374. https://doi.org/10.1016/S0022-3093(05)80645-3.

STAR★METHODS

KEY RESOURCES TABLE

REAGENT or RESOURCE	SOURCE	IDENTIFIER
Chemicals, peptides, and recombinant proteins		
N,N-Dimethylformamide	Xilong Scientific Co., Ltd., China	CAS:110-70-3
Ethanol	Peking Reacgent Co., Ltd., China	CAS:64-17-5
UHP Ar, 99.999%	Jinghui Gas Co., Ltd., China	CAS: 7440-37-1
Other		
Polyamic acid	Changzhou Sunchem High Performance Polymer Co., Ltd, China	20 wt% with intrinsic viscosity of 0.18 $dL \cdot g^{-1}$

RESOURCE AVAILABILITY

Lead contact

Further information and requests for resources and reagents should be directed to and will be fulfilled by the lead contact, Guotong Qin (qingt@buaa.edu.cn).

Materials availability

All unique/stable materials generated in this study are available from the lead contact with a completed Materials Transfer Agreement. This study did not generate new unique materials.

Data and code availability

- The authors declare that the data supporting the findings of this study are available within the article and the supplemental information.
- This article does not report original codes.
- Any additional information required to reanalyze the data reported in this article is available from the lead contact request.

EXPERIMENT MODEL AND SUBJECT DETAILS

No experimental model exists for this work.

The synthesis method.

Preparation of films

The process of preparing PI film is shown in Figure S5. Polyamic acid (PAA, 20 wt%, intrinsic viscosity of 0.18 $dL \cdot g^{-1}$, supplied by Changzhou Sunchem High Performance Polymer Co., Ltd.) was used as the starting material to prepare porous gel by a phase separation approach. PAA was diluted with N,N-Dimethylformamide (DMF, A.R., Xilong Scientific Co., China) to obtain 10 wt% PAA. The viscous solution was dispersed on a clean glass plate using an automatic coating machine (Sheen 1132N, UK) with an applicator of width 100 mm and gap size 250 μm (step 1) to obtain PAA film. The film was immersed in a non-solvent (water/ethanol), phase separation occurred with the formation of a wet porous film, which was then transferred to a water bath to fully remove the residual DMF as well as ethanol from the film pores (step 2). The PI film was obtained by drying and thermal imidization of a wet porous PAA film (step 3). The dried film was thermally imidized under an argon atmosphere by raising the temperature at $5^{\circ}C \cdot min^{-1}$ to 300°C, heating for 1 hour (h), further rising to 400°C, and heating for another hour. The Scheme 1 shows the change of the chemical structure of the films during the thermal imidization.

Effects of the coagulation composition on the structure of PI films

Polyamic solution was cast on a glass plate and then immersed into a coagulation bath with mixture of water and ethanol, leading to a wet PAA film. The PAA film was then removed from the coagulation bath and

dried at ambient pressure and temperature followed a thermal imidization to get a PI film. The ethanol content in coagulation bath strongly affects the pore structure of the PI film (Figure S1). From Figures S1A–S1K the ethanol content in coagulation was increased in increments of 10%. As shown in Figure S1A, when pure water was used as non-solvent. The obtained PI film showed relative dense skin with reduced number of small pores whereas the cross-section showed hierarchical micro-nano porous structure. With the increase of the ethanol in coagulation bath, the macro void was reduced gradually (Figures S1B and S1C). When the ethanol content reached 30%, the macro void disappeared and the film became homogeneously porous with interconnected pores (Figure S1D). Further increase of ethanol in coagulation resulted in highly porous surface layer and decreased pore size whereas the pores gradually changed to more and more closed from highly interconnected structure (Figures S1D–S1H). The smallest pores were shown in the film from a coagulation bath with 70% ethanol (Figure S1H). When the ethanol in coagulation bath was increased to 80–100%, the pores in PI film was enlarged and the pore walls became thicker.

Thermogravimetric stability

The weight loss of PAA films from room temperature to 150°C was corresponding to the evaporation of solvent entrapped inside the pores. Above 150°C, the weight decrease was mainly related with the loss of water, released from the imidization process. On the contrary, PI films display a very stable profile (Figure S2).

Heat transferring property of the aerogel PI films

The total thermal conductivity is given by (Figure 2)

$$\lambda_t = \lambda_s + \lambda_r + \lambda_g \quad \text{(Equation 1)}$$

where λs, λr, and λg denotes the solid, radiative, and gas-phase conductivity values, respectively. The solid thermal conductivity λs, based on phonon conductivity along with solid PI walls, is closely related to the porosity of the material. The value of λs for an aerogel strongly depends on its density ρ. The porosity of the film decreased the solid thermal conductivity base on phonon conductivity. Solid thermal conductivity can be calculated using

$$\lambda_s = \lambda_{s,s}\left(\rho v / p_s v_s\right) \quad \text{(Equation 2)}$$

where $\lambda_{s,s}$ is solid thermal conductivity for basic materials, v is the velocity of phonon, v_s is the velocity of phonon for basic materials, ρ_s is the true density of the material, ρ is the apparent density of the film. Density ρ is related with the porosity while$v$ is related with the vibration of phonon for heat transfer, which is determined by the pathway for conduction.

The thermal conductivity of the gas phase in an aerogel is given by

$$\lambda_g = (\lambda_0 \delta / 1 + aKn) \quad \text{(Equation 3)}$$

where λ_0 is the thermal conductivity of the gas in the pores, δ is the porosity, a is a constant depending on the gas species (about 2 for air), and K_n is the Knudsen number, which is the ratio of the mean free path of the gas to the pore size.

The radiative thermal conductivity is given by

$$\Lambda_r = \left(16n\sum t_r^3\right) \Big/ \left(3\rho K_s / \rho_s\right) \quad \text{(Equation 4)}$$

The weight loss, area shrinkage and thickness change before and after drying or imidization

As expected, the wet PAA films experienced a high weight loss and area shrinkage after drying. It is not surprising to observe that the weight loss and area shrinkage of PAA films after imidization was much reduced and the weight was maintained relatively stable (Table S2).

METHOD DETAILS

Thermal conductivity measurement

The thermal conductivity was measured using a Hot Disk TPS 2500 S apparatus. The error bars were generated by testing different samples with same experiment condition (Figure 3).

Tensile performance measurement

The tensile performance was tested using an AGS-X 1KN universal test machine (Shimadzu Corporation, Japan) at a speed of 1 mm•min^{-1} (Figure 3).

Surface morphology

The surface morphology of the polyimide films was investigated by a field emission scanning electron microscope (SEM, JSM-7500F, JEOL Ltd., Japan) (Figures 1 and S1).

BET surface area, pore volume, and pore size measurement

The BET surface area, pore volume, and pore size of the polyimide films were characterized using a Micrometrics ASAP 2020 adsorption instrument at 77 K (Figure S4 and Table 1).

Infrared thermal images

For the thermal insulation performance test, the infrared thermal images were taken by a Testo (865) camera. The working distance was about 30 cm. The temperatures of samples were monitored and recorded to 40°C with hot stage (Figure S3).

Thermogravimetric analysis

The thermogravimetric analysis of the PAA and PI films were analyzed using PerkinElmer TGA 8000 thermogravimetric analyzer at a heating rate of 10°C•min^{-1} from 50°C to 400°C under a nitrogen atmosphere (Figure S2).

QUANTIFICATION AND STATISTICAL ANALYSIS

Origin 8 to perform data processing on thermal conductivity, tensile stretch and stretch module data, thermogravimetric, nitrogen adsorption isotherms and pore size distributions (Figures 3, S2, and S4).